Magnetic and charge instabilities in vanadium-based topological kagome metals

Hai-Yang Ma [1,2] Jia-Xin Yin,[3] M. Zahid Hasan,[3,4,5] and Jianpeng Liu [1,2,*]

[1]*School of Physical Science and Technology, ShanghaiTech University, Shanghai 201210, China*
[2]*ShanghaiTech laboratory for topological physics, ShanghaiTech University, Shanghai 201210, China*
[3]*Laboratory for Topological Quantum Matter and Advanced Spectroscopy (B7), Department of Physics, Princeton University, Princeton, New Jersey 08544, USA*
[4]*Princeton Institute for Science and Technology of Materials, Princeton University, Princeton, New Jersey 08544, USA*
[5]*Materials Sciences Division, Lawrence Berkeley National Laboratory, Berkeley, California 94720, USA*

(Received 10 January 2022; revised 25 July 2022; accepted 5 October 2022; published 14 October 2022)

Vanadium-based topological kagome metals AV_3Sb_5 (A = K, Rb, Cs) have drawn great attention recently due to the discoveries of charge order, nematic phase, time-reversal symmetry breaking, and superconductivity. In this work, we study the Fermi-surface instabilities of topological kagome metals AV_3Sb_5 (A = K, Rb, Cs) in all the charge-orbital-spin channels based on first principles calculations, and provide a first principles theory for the current-loop state in this class of materials. After comprehensive analysis of the interaction-renormalized generalized susceptibility tensor combined with unrestricted Hartree-Fock calculations, we find that the leading instability modes at the Fermi surface are three spin magnetic modes at Γ point, giving rise to ferromagnetism within the kagome plane with small magnetization on the V atoms. We further show that counter-propagating current loops within the kagome plane can be generated due to the interplay between spin magnetism and spin-orbit coupling, and the current pattern is consistent with recent muon spin spectroscopy measurements. Moreover, some other puzzling experiments in this system such as the giant anomalous Hall effect and nematicity can also be explained from our results.

DOI: 10.1103/PhysRevB.106.155125

I. INTRODUCTION

Quantum materials with layered kagome structures are of great interest due to the frustrated lattice geometry, which can give rise to interesting noninteracting band structures with both flat bands and Dirac cones [1]. The nontrivial Berry phase associated with the Dirac fermions and the vanishing kinetic energy of the flat bands make the kagome lattice system an ideal platform to study the interplay between band topology and strong electron-electron (*e-e*) correlations, which can lead to various exotic quantum states [2–12]. Recently, vanadium-based layered kagome materials AV_3Sb_5 (A=K, Rb, Cs) have been successfully synthesized [13,14], which exhibit various intriguing properties including charge density wave states [15–34], the signature of time-reversal symmetry breaking [14,15,35–37] and nematicity [38], as well as unusual superconductivity [34,39–54].

These experimental observations have boosted intensive theoretical interest [54–66]. First principles calculations reveal that the band structures of AV_3Sb_5 are topologically nontrivial with nonzero $\mathbb{Z}_2$ indices and Dirac-like linear dispersions, and there are multiple van Hove singularities near the Fermi level [41]. Various instability modes in the interaction-driven Fermi-surface nesting scenario have been predicted based on continuum model Hamiltonian around saddle points of band dispersions [55] or simplified lattice model Hamiltonians [56,57,60].

Recent phonon calculations indicate the presence of unstable phonon modes in the system, which suggests that the CDW phase may be driven by electron-phonon couplings and phonon instabilities [29,62–64,67]. Density functional theory (DFT) calculations also indicate multiple Fermi surfaces which have significant contributions from all the V 3*d* and Sb 5*p* orbitals [29,41,63]. Given such complex Fermi surfaces and the multiple sublattice, orbital, and spin degrees of the system, *e-e* interactions may lead to complicated symmetry-breaking states in the charge-sublattice-orbital-spin space, which is difficult to be fully captured by any simplified tight-binding model including only one orbital at each V site, or by any continuum model centered at one particular high-symmetry point in the Brillouin zone. Therefore, in order to unambiguously identify the leading Fermi-surface instabilities and shed light on the nature of the charge and magnetic properties in this system, we study the interacting ground states of the systems based on realistic Wannier tight-binding models generated from first principles calculations, and provide a first principles theory for the time-reversal-breaking current-loop states in this class of materials.

Specifically, we first calculate the generalized two-particle susceptibility tensor defined the charge-sublattice-orbital-spin space based on realistic 60-band Wannierized tight-binding models generated from first principles DFT calculations, including the effects of both on-site and intersite *e-e* Coulomb interactions as treated by generalized random phase ap-

*liujp@shanghaitech.edu.cn

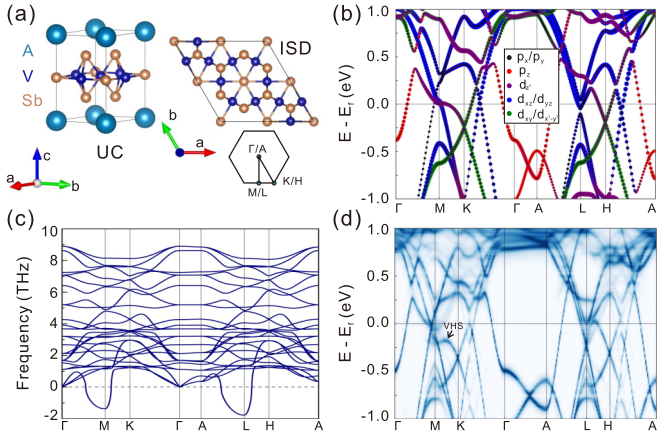

FIG. 1. Geometric, electronic, and dynamic properties of AV_3Sb_5 (A = K, Rb, Cs). (a) Lattice structures of the normal phase and the CDW phase. (b) Band structures for the normal phase of RbV_3Sb_5 projected onto V d and Sb p orbitals. (c) Phonon spectrum for the normal phase of RbV_3Sb_5. (d) Unfolded spectral function of the CDW phase of RbV_3Sb_5, where the new von Hove singularity (VHS) is marked by an arrow.

proximation [68,69]. Taking the leading eigenmodes of the generalized susceptibility tensor as initial ansatzs, we further perform unrestricted self-consistent Hartree-Fock calculations for both pristine structure, $2 \times 2 \times 1$ inverse-star-of-David (ISD) supercell, and a $2 \times 2 \times 2$ supercell, including both Kanamori-type on-site interactions for V $3d$ orbitals, as well as V-Sb and V-V intersite Coulomb interactions. The nonlocal exchange effects are treated exactly. Through these calculations, we find that the ground-state manifold consists of three nearly degenerate spin magnetic states. The inclusion of intersite Coulomb interactions would significantly suppress the spin magnetism, leading to weak spin magnetization $\sim 0.06\,\mu_B$ per V atom. Counter-propagating current loops (with current amplitudes ~ 100 nA) can be generated in the magnetic states as a result of spin-orbit coupling, giving rise to staggered orbital magnetic fluxes threaded through the kagome plane in both the $2 \times 2 \times 1$ ISD supercell and the $2 \times 2 \times 2$ supercell. We further propose that an intralayer ferromagnetic and interlayer antiferromagnetic state in the $2 \times 2 \times 2$ supercell is the candidate for the time-reversal breaking nematic state observed in experiments [15,35,36,38].

II. PRELIMINARIES

The AV_3Sb_5 (A = K, Rb, Cs) system crystallizes in a layered kagome lattice structure as shown in Fig. 1(a). We first perform first-principle calculations to study its electronic properties. First principles calculations are performed within the framework of density functional theory as implemented in Vienna *ab initio* simulation (VASP) package. The projector-augmented wave potential is adopted with the plane-wave energy cutoff set at 400 eV [70]. The exchange-correlation functional of the Perdew-Burke-Ernzerhof (PBE-GGA) type is used for the calculations [71,72]. $8 \times 8 \times 4$ and $6 \times 6 \times 4$ $\mathbf{k}$ meshes are used for the the calculations of the pristine lattice structure and the inverse star-of-David (ISD) $2 \times 2 \times 1$ structure, respectively. We take the lattice constants of the AV_3Sb_5 (A = K, Rb, Cs) from Ref. [13].

In Fig. 1(b) we show the DFT band structure of RbV_3Sb_5 projected onto V $3d$ orbitals and Sb $5p$ orbitals in the pristine lattice structure including spin-orbit coupling (SOC). Clearly there are Dirac-like dispersions near K and H points contributed by V $3d$ orbitals, van Hove singularities near M point contributed by both V $3d$ and Sb $5p$ orbitals, as well as electron pockets centered at Γ contributed by Sb $5p$ orbitals. Such complicated Fermi surfaces and orbital characters make it difficult to realistically describe the electronic structure of this system using any simplified lattice model or continuum model. In Fig. 1(c) we present the phonon dispersions calculated by DFT using the frozen-phonon method with a $3 \times 3 \times 1$ supercell, where we see two unstable phonon modes around M and L points [29,62–64]. A linear combination of the unstable modes at the three equivalent M points result in an inverse-star-of-David structure with $2 \times 2 \times 1$ supercell as shown in the right panel of Fig. 1(a). New van Hove singularities emerge below the Fermi level as a result of the lattice deformation in the $2 \times 2 \times 1$ supercell [29] as shown by the spectral function unfolded to the original primitive Brillouin zone in Fig. 1(d).

III. FERMI SURFACE INSTABILITIES

The presence of van Hove singularities both in the pristine and in the ISD structures indicate that the noninteracting Fermi surfaces may be unstable to *e-e* Coulomb interactions. In order to study the interaction effects on the complicated Fermi surfaces with diverse orbital characters as shown in Fig. 1(b), we first construct a realistic tight-binding model in the Wannier-function basis using the Wannier90 code package [73]. To be specific, the Bloch functions generated from DFT calculations are projected onto 60 spinor Wannier functions (for each pristine primitive cell) including all the V $3d$ orbitals and Sb $5p$ orbitals, from which we obtain the following Wannier tight-binding model denoted by H_0:

$$H_0 = \sum_{i\alpha\sigma, j\beta\sigma'} h_{i\alpha\sigma, j\beta\sigma'}\, \hat{c}^{\dagger}_{i\alpha\sigma}\, \hat{c}_{j\beta\sigma'}, \tag{1}$$

where the sets of indices $\{i, j\}$, $\{\alpha, \beta\}$, and $\{\sigma, \sigma'\}$ denote, in turn, all the V and Sb atomic sites, orbitals, and spin degrees of freedom, and $h_{i\alpha\sigma, j\beta\sigma'}$ denotes the real-space hopping amplitude including spin-orbit coupling effects. $\hat{c}^{\dagger}_{i\alpha\sigma}$ and $\hat{c}_{j\beta\sigma'}$ are the electron creation and annihilation operators. We include the on-site multi-orbital Coulomb interactions of the Kanamori type for the V $3d$ orbitals [74,75],

$$\begin{aligned} H_{\mathrm{K}} = {} & U \sum_{i,\alpha} \hat{n}_{i\alpha\uparrow}\hat{n}_{i\alpha\downarrow} + U' \sum_{i,\alpha<\beta,\sigma,\sigma'} \hat{n}_{i\alpha\sigma}\hat{n}_{i\beta\sigma'} \\ & - J_{\mathrm{H}} \sum_{i,\alpha<\beta,\sigma,\sigma'} \hat{c}^{\dagger}_{i\alpha\sigma}\hat{c}_{i\alpha\sigma'}\hat{c}^{\dagger}_{i\beta\sigma'}\hat{c}_{i\beta\sigma} \\ & + J_{\mathrm{P}} \sum_{i,\alpha<\beta,\sigma} \hat{c}^{\dagger}_{i\alpha\sigma}\hat{c}^{\dagger}_{i\alpha-\sigma}\hat{c}_{i\beta\sigma}\hat{c}_{i\beta-\sigma}, \end{aligned} \tag{2}$$

where U and U' are the intraorbital and interorbital direct Coulomb interactions. J_{H} and J_{P} denote the Hunds' coupling and pair hoppings, respectively, and $\hat{n}_{i\alpha\sigma} = \hat{c}^{\dagger}_{i\alpha\sigma}\hat{c}_{i\alpha\sigma}$ is the

density operator. We let $U' = U - J$ and $J_P = 0$ such that Eq. (2) has full rotational invariance [75]. We further consider the density-density intersite interactions between the neighboring V-Sb sites and V-V sites; the interaction amplitudes are denoted by V and W respectively,

$$H_{\text{V-Sb}} = V \sum_{\langle ij \rangle} \sum_{\alpha\beta\sigma\sigma'} \hat{c}^{\dagger}_{i\alpha\sigma} \hat{c}^{\dagger}_{j\beta\sigma'} \hat{c}_{j\beta\sigma'} \hat{c}_{i\alpha\sigma},$$
$$H_{\text{V-V}} = W \sum_{\langle\langle ij \rangle\rangle} \sum_{\alpha\beta\sigma\sigma'} \hat{c}^{\dagger}_{i\alpha\sigma} \hat{c}^{\dagger}_{j\beta\sigma'} \hat{c}_{j\beta\sigma'} \hat{c}_{i\alpha\sigma}, \tag{3}$$

where "$\sum_{\langle ij \rangle}$" means a summation over all the first-neighbor V-Sb sites (including both intralayer ones and interlayer ones), and the symbol "$\sum_{\langle\langle ij \rangle\rangle}$" means summing over all the inplane nearest neighbor V-V sites. In this work, V and W are treated as two free parameters which vary from 0 to 1 eV. The full Hamiltonian is then $H_0 + H_K + H_{\text{V-Sb}} + H_{\text{V-V}}$. We set the onsite interaction parameters $U = 3.6$ eV and $J = J_H = 0.72$ eV, and the intersite interaction parameters (if applicable) $V = 1.0$ eV, and $W = 0.2$ eV throughout this paper. We have also performed RPA+Hartree-Fock calculations for $3.4\,\text{eV} \leqslant U \leqslant 5.4\,\text{eV}$ and $0 \leqslant V \leqslant 1.5\,\text{eV}$, all of which lead to qualitatively the same ground state [76].

As discussed above, the system has a quite complicated primitive cell with multiple sublattice, orbital, and spin degrees of freedom. For the 60-band tight-binding model, there are 3600 independent matrix elements of the density operator $\rho_{\mu,\nu} = \langle \hat{c}^{\dagger}_{\mu} \hat{c}_{\nu} \rangle$ (with μ, ν being composite indices referring to all the sublattice, orbital, and spin degrees of freedom), each of which can be considered as an "order parameter" that break certain symmetries of the system and bring about Fermi surface instability. The actual ground state is characterized by a linear combination of the density matrix elements, which is difficult to guess *a priori* for the *ab initio* DFT+U or hybrid-functional type calculations due to such complexity. Therefore, in order to find the leading Fermi-surface instability mode, we propose to calculate the interaction-renormalized generalized susceptibility tensor defined in the sublattice-orbital-spin space, the tensor element of which is denoted as $\chi(\mathbf{q})_{\mu\nu,\mu'\nu'}$. Consider a field $\mathbf{A}^{\kappa}$ that is only coupled to (or "parallel" to) the κth eigenmode $u^{\kappa}_{\mu\nu}(\mathbf{q})$ of the susceptibility tensor, i.e., $\mathbf{A}^{\kappa}(\mathbf{q}) \sim u^{\kappa}_{\mu\nu}(\mathbf{q})$, then the system would respond to such a field along the eigenvector direction via $\delta\rho_{\mu\nu}(\mathbf{q}) \sim \lambda^{\kappa}(\mathbf{q}) u^{\kappa}_{\mu\nu}(\mathbf{q})$, where $\lambda^{\kappa}(\mathbf{q})$ and $u^{\kappa}_{\mu\nu}(\mathbf{q})$ are the eigenvalues and eigenvectors of the susceptibility tensor $\chi(\mathbf{q})$. If any of the eigenmodes has a diverging eigenvalue $\lambda(\mathbf{q})^{\kappa}$, the system would develop a spontaneous order parameter characterized by the diverging eigenmode $u^{\kappa}_{\mu\nu}(\mathbf{q})$ upon the application of an infinitesimal field, and would enter a spontaneous symmetry-breaking state through a continuous transition [77–79].

The dynamical generalized susceptibility tensor of a nonsystem at wavevector $\mathbf{q}$ and frequency ω is expressed as

$$\chi^{0}_{\mu\nu,\mu'\nu'}(\mathbf{q},\omega) = \int_{\text{BZ}} \frac{\Omega\, d^3\mathbf{k}}{(2\pi)^3} \sum_{m,n} \frac{f(E_{n,\mathbf{k}}) - f(E_{m,\mathbf{k}+\mathbf{q}})}{E_{m,\mathbf{k}+\mathbf{q}} - E_{n,\mathbf{k}} - \hbar(\omega + i\delta)} \psi^{*}_{\mu,n}(\mathbf{k}) \psi_{\nu,m}(\mathbf{k}+\mathbf{q}) \psi_{\mu',n}(\mathbf{k}) \psi^{*}_{\nu',m}(\mathbf{k}+\mathbf{q}), \tag{4}$$

where μ, ν are composite indices referring to the sublattice, orbital, and spin degrees of freedom, m and n are the band indices, and Ω is the volume of the unit cell. $f(E_{n,\mathbf{k}})$ is the Fermi-Dirac distribution function at zero temperature, with $E_{n,\mathbf{k}}$ denoting the band energy of the nth band at wavevector $\mathbf{k}$, and $\psi_{\mu,n}(\mathbf{k})$ is the corresponding eigenfunction in the basis of the Fourier-transformed Wannier functions. In order to study the ground state Fermi-surface instabilities driven by electron-electron Coulomb interactions, here we only consider the static susceptibility at zero frequency ($\omega = 0$), and study the wavevector ($\mathbf{q}$) dependence of the susceptibility tensor. A linear tetrahedra interpolation method is applied for the integration of the $\mathbf{k}$ points over the first Brillouin zone [80]. A $50 \times 50 \times 20$ $\mathbf{k}$ mesh is already fine enough for the numerical convergence in calculating the bare susceptibility. The summation over the band indices is restricted to the 10 (including spin) bands near the Fermi level.

The effects of Coulomb interactions on the generalized susceptibility tensor are treated within random phase approximation (RPA), including effects of both direct and exchange interactions as described by the bubblelike and ladderlike Feynmann diagrams for the two-particle correlation function. The wavevector dependent intersite exchange interaction is replaced by the wavevector-averaged one in the susceptibility calculation, i.e., a $\mathbf{k}$ independent exchange interaction vertex is adopted. We have included the on-site multi-orbital Kanamori interactions for the V $3d$ orbitals as given by Eq. (2), the first neighbor Sb-V Coulomb interactions whose amplitude is denoted by V, as well as the inplane nearest neighbor V-V interactions whose amplitude is denoted by W, as given by Eq. (3). All these Coulomb interaction terms (after Fourier transform) can be expressed in matrix form denoted by $\mathbb{U}$, which include both direct and exchange interactions, then the RPA generalized susceptibility tensor is expressed as

$$\hat{\chi}(\mathbf{q}) = \hat{\chi^{0}}(\mathbf{q}) \cdot (\mathbb{1} + \mathbb{U}(\mathbf{q}) \cdot \hat{\chi}^{0}(\mathbf{q}))^{-1}, \tag{5}$$

where $\hat{\chi}(\mathbf{q})$ and $\hat{\chi^{0}}(\mathbf{q})$ refer to the RPA and bare susceptibility tensor (at wavevector $\mathbf{q}$), respectively, each of which is a 3600×3600 matrix. $\hat{\chi^{0}}(\mathbf{q})$ is defined in Eq. (4). The interaction matrix $\mathbb{U}(\mathbf{q})$ is also a 3600×3600 matrix defined in the same two-particle Wannier basis as $\hat{\chi^{0}}(\mathbf{q})$. The "$\cdot$" in Eq. (5) denotes a matrix product operation.

Following the above argument, we calculate the generalized susceptibility tensor for the AV_3Sb_5 (A = K, Rb, Cs) systems. For clarity's sake, in main text we only present the results for RbV_3Sb_5, and the results of the other two compounds are given in the Supplemental Material [76]. In Fig. 2(a) we present the 10 eigenmodes with maximal eigenvalues of the RPA susceptibility as a function of the wavevector $\mathbf{q}$, with on-site interaction only and the intersite interactions being temporarily turned off. We see that there are three diverging

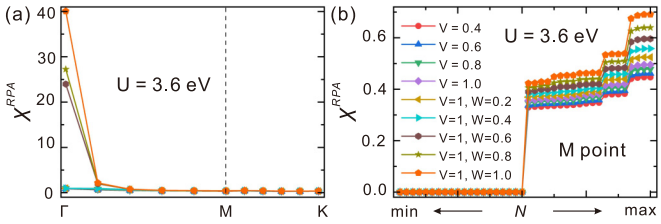

FIG. 2. RPA susceptibility of the pristine RbV_3Sb_5. (a) Eigenvalues of the generalized RPA susceptibility tensor (with on-site interaction only), plotted along a high-symmetry $\mathbf{q}$ path. Only the 10 leading eigenvalues are shown. (b) The eigenvalues of the RPA susceptibility at M point for different V-Sb (V) and V-V (W) intersite interaction strengths.

modes only at Γ point, which turn out to be three spin magnetic modes. The inclusion of intersite interactions does not change the diverging nature of the three spin ferromagnetic modes. On the other hand, since the system undergoes a CDW transition forming a $2 \times 2 \times 1$ ISD structure around 100 K, we also check the eigenmodes of the RPA susceptibility tensor at M points, and do not find notable unstable modes. We further include V-Sb and V-V intersite interactions, and find that the eigenvalues of the susceptibility tensor at M points only increase by small amounts due to the inclusion of intersite interactions, as clearly shown in Fig. 2(b). Therefore, the CDW phase is likely driven by strong electron-phonon couplings and phonon instability instead of e-e interactions.

IV. SYMMETRY-BREAKING GROUND STATES

In order to verify the conclusions obtained from the susceptibility calculations, and to unambiguously determine the symmetry-breaking ground states of the systems, we further perform unrestricted self-consistent Hartree-Fock (HF) calculations including both the on-site Kanamori interactions and the intersite interactions based on the first principles Wannier tight-binding models [76]. We first perform HF calculations for the pristine primitive cell, and we take the three leading instability modes at Γ point [Fig. 2(a)] as initial ansatz for the density matrices. The HF ground states turn out to be three spin ferromagnetic states with the magnetizations primarily pointing along the crystalline x, y, and z directions with slight cantings [76]. With on-site interactions only, the spin magnetization is as large as $\sim 0.6\,\mu_B$ per V atom. Real-space current loops are generated in the ferromagnetic states by virtue of SOC, and the current amplitudes ~800 nA. We note that although the exact exchange would give rise to spontaneous symmetry breaking states in the Hartree-Fock theory, the correlation effects of e-e interactions have been neglected. The latter may suppress the spin magnetization due to the enhanced local spin fluctuations [81].

The intersite current can be calculated as follows. The rate of change of charge density at an atomic site j is expressed as

$$\frac{dn_j}{dt} = -\frac{2}{\hbar}\mathrm{Im}\sum_{\alpha\alpha' j'} \rho_{\alpha j,\alpha' j'}(\mathbf{R}) H_{\alpha' j',\alpha j}(-\mathbf{R}), \qquad (6)$$

where $\{\alpha, \alpha'\}$ refers to the orbital indices and $\{j, j'\}$ refers to the site (or sublattice) indices. $\hat{n}_j = \sum_\alpha |\phi_{\alpha j}\rangle\langle\phi_{\alpha j}|$ is the electron number operator in the Wannier basis, and $\hat{\rho} = \sum_{n,\mathbf{k}} |\psi_{n,\mathbf{k}}\rangle\langle\psi_{n,\mathbf{k}}|\theta(E_F - E_{n,\mathbf{k}})$ (n is the band index, $\theta(E_F - E_{n,\mathbf{k}})$ is the step function) is the density operator in the Bloch basis. Here $\rho_{\alpha j,\alpha' j'}(\mathbf{R})$ is expressed as $\rho_{\alpha j,\alpha' j'}(\mathbf{R}) = \sum_{\mathbf{k}} e^{-i\mathbf{kR}} \rho_{\alpha j,\alpha' j'}(\mathbf{k})/N$, and $H_{\alpha j,\alpha' j'}(-\mathbf{R}) = \sum_{\mathbf{k}} e^{i\mathbf{kR}} H_{\alpha j,\alpha' j'}(\mathbf{k})/N$. We define the intersite current between site j' and j as $I_{jj'} = -(2/\hbar)\mathrm{Im}\sum_{\alpha,\alpha'} \rho_{\alpha j,\alpha' j'}(\mathbf{R})\, H_{\alpha' j',\alpha j}(-\mathbf{R})$.

The inclusion of intersite interactions, e.g., with $V = 1$ eV and $W = 0$, would significantly suppress the spin ferromagnetism, resulting in a spin moment $\sim 0.06\,\mu_B$ per V atom. Once the intersite interaction is taken into account, charges tend to transfer from the V to the Sb sites to minimize the intersite Coulomb energy, resulting in a charge occupation ~0.3 per V atom for $V = 1$eV, which is reduced by a factor of six compared with the case when $V = 0$. As a result, the spin magnetization driven by the on-site interactions of V $3d$ orbitals is significantly diminished. We also note that the magnetic moments of V atoms can be further suppressed by local dynamical fluctuation effects as discussed in Ref. [81]. Such small magnetic moments and the small anisotropy energy can explain why no long-range magnetic order has been observed in this class of material so far.

A. Current-loop state in 2 × 2 × 1 CDW phase

We have also performed HF calculations for the $2 \times 2 \times 1$ ISD lattice structure with a realistic tight-binding model including 240 Wannier orbitals, including both the on-site and intersite interactions, and the nonlocal exchange effects are treated exactly. We take the three spin ferromagnetic modes at Γ point and four leading modes at M point as our initial ansatzs for the density matrices in the HF calculations. The ground states, again, involve three nearly degenerate spin ferromagnetic states with their magnetizations primarily pointing along the crystalline x, y, and z directions, which are denoted as FM_x, FM_y, and FM_z states, respectively. The three FM states are competing with each other with the energy difference ~0.01 meV. Similar to the case of pristine primitive cell, the magnetizations in the ISD structure are on the order of $1\,\mu_B$ per V if only on-site interactions are included, and can be suppressed by one order of magnitude due to the intersite interaction effects. Interestingly, in the ISD structure, the magnetization distribution is inhomogeneous within the ISD primitive cell: the spin magnetizations are mostly concentrated at the six V atoms forming two contracted kagome triangles, as schematically shown in Fig. 3(b) for the FM_z phase.

Current loops are generated in the intralayer FM state of the ISD structure due to SOC effects. The current-loop patterns in the three FM states are shown in Fig. 3(a) for the FM_y, FM_z, and FM_x states respectively. For example, for the FM_z state, there are three current loops: two of them are counterclockwise circulating around the two kagome triangles, and the other one is clockwise circulating around the hexagon, with the current amplitudes ~80 nA (for intersite interaction amplitude $V = 1$ eV). It is worthwhile to note that in the ISD structure there are always chiral current loops within the V kagome plane for all the three ferromagnetic states. This is because in the FM_x and FM_y states, the magnetizations have

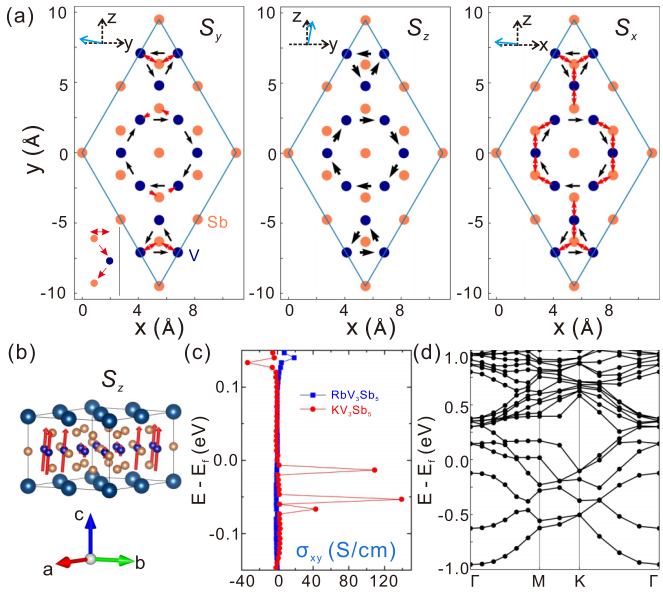

FIG. 3. Properties of the spin ferromagnetic states in the $2 \times 2 \times 1$ ISD structure including both on-site interaction and V-Sb intersite interaction (V), with $V = 1.0$ eV. (a) Schematic illustration of the intersite currents for the three spin ferromagnetic states of RbV_3Sb_5; (b) magnetic structure of the FM_z phase, with the arrows denoting the spin magnetization at different sites; (c) calculated anomalous Hall conductivity of the FM_z phase; (d) Hartree-Fock band structures of the FM_z phase.

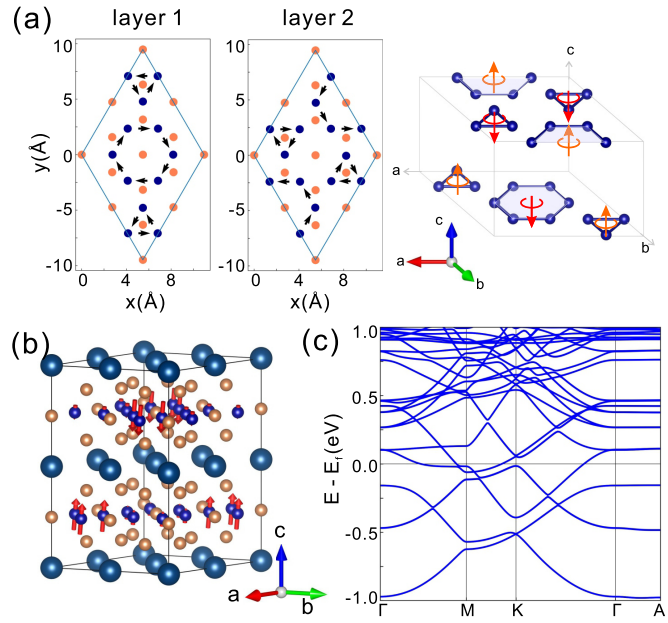

FIG. 4. Properties of the current-loop states in the $2 \times 2 \times 2$ CDW phase including both on-site and V-Sb intersite interactions (with $V = 1.0$ eV). (a) Schematic illustration of the current loops in the first and second layer in the A-type antiferromagnetic state, where the left panel is from our calculations and the right panel is deduced from muon spin relaxation measurements reported in Ref. [36]. (b) Magnetic structure of the A-type antiferromagnetic phase, with the arrows denoting the spin magnetizations. (c) The Hartree-Fock band structures.

cantings along the crystalline z direction with canting angle $\sim 10^\circ$ [see Fig. 3(a)], thus generating in-plane current loops due to SOC effects. This implies that even if there are strong real-space magnetic fluctuations due to the quasi-degeneracy among the FM_x, FM_y, and FM_z states such that the system hardly has long-range ferromagnetic order, there are still in-plane chiral current loops.

We have further calculated the intrinsic anomalous Hall conductivity (AHC) of the weak FM state in the ISD structure, which is very small $\sim 1 - 20$ S/cm in the FM_z state for RbV_3Sb_5 as shown by the blue line in Fig. 3(c). The experimentally measured giant AHC of KV_3Sb_5 thus arise from skew scatterings [14], which may be induced by the strong real-space magnetic fluctuations [82] by virtue of the near degeneracy of the three ferromagnetic states. Ref. [14] also reported the intrinsic contribution to AHC of KV_3Sb_5, which is $\sim 10^2$ S/cm, two orders of magnitude weaker than the skew-scattering contribution [14]. In order to directly compare our theory with the experiment, we have also calculated the intrinsic AHC in the FM_z phase of KV_3Sb_5 in the ISD structure, as shown by the red lines in Fig. 3(c). We see that the maximal value ~ 140 S/cm, which is qualitatively consistent with the experimentally measured value. In Fig. 3(d), we show the calculated HF band structures of the $2 \times 2 \times 1$ ISD structure (plotted in the supercell Brillouin zone) with intersite interaction $V = 1.0$ eV, from which we see a strong renormalization effect on the electronic structures due to the inclusion of intersite interactions. Notably, the Fermi surfaces are mostly contributed by two bands with nearly compensated electron-type and hole-type carriers due to time-reversal breaking.

B. Current-loop state in 2 × 2 × 2 CDW phase

As discussed in Ref. [67], the ground-state lattice structure in the CDW phase may have additional structural modulation along the z direction, forming a $2 \times 2 \times 2$ supercell with the two neighboring $2 \times 2 \times 1$ ISD planes being mutually shifted by one pristine lattice vector. Our calculations indicate that the magnetic ground state in such a $2 \times 2 \times 2$ CDW phase is an "A-type" antiferromagnetic state with intralayer ferromagnetism and interlayer antiferromagnetism as shown in Fig. 4(b). The A-type antiferromagnetism results in counter-propagating current loops and staggered orbital flux pattern along the z axis, as shown in Fig. 4(a). This is perfectly consistent with the flux pattern deduced from recent muon spin relaxation measurements at temperatures $\lesssim 30-40$ K [35,36] as schematically shown in the right panel of Fig. 4(a). Moreover, as the A-type antiferromagnetic state in the $2 \times 2 \times 2$ supercell breaks C_{3z} symmetry, here we propose it as the candidate for the nematic state observed in experiments [38]. In Fig. 4(c) we also show the HF band structures of the $2 \times 2 \times 2$ supercell in the antiferromagnetic state. The Fermi surfaces have been strongly reconstructed, which consist of nearly compensating electron and hole pockets. These results imply that there are two kinds of instabilities in the AV_3Sb_5 (A = K, Rb, Cs) system, the first one is the CDW instability driven by electron-phonon couplings, and the other is the magnetic instability as marked by the emergence of the giant anomalous Hall effect and the onset of muon spin relaxation signal. These two kinds of instabilities could be coupled together if both *e-e*

Coulomb interactions and electron-phonon interactions are taken into account properly, leading to a joint phonon-electron instability mode [83], and may give rise to a time-reversal breaking CDW state.

V. DISCUSSIONS

In this work we have comprehensively studied the magnetic and charge instabilities of the AV_3Sb_5 (A = K, Rb, Cs) system based on first principles calculations including effects of both on-site and intersite Coulomb interactions. Results from both RPA susceptibility calculations and unrestricted Hartree-Fock calculations indicate that the leading Fermi-surface instabilities are three nearly degenerate intralayer spin ferromagnetic modes, and the spin magnetization can be strongly suppressed by intersite interactions. Current loops can be generated in the spin magnetic states by virtue of SOC, giving rise to staggered orbital magnetic fluxes. We further propose that the time-reversal breaking nematic state observed in experiment is an intralayer ferromagnetic and interantiferromagnetic state in the $2 \times 2 \times 2$ supercell breaking C_{3z} symmetry. Our results shed light on the nature of the elusive correlated and topological states in the kagome metal AV_3Sb_5 (A = K, Rb, Cs) system, and provide a first principles theory for the current-loop state in these systems. The first principles methodology presented in this work can be widely applied in various complex metallic systems with both strong Coulomb interactions and spin-orbit coupling, which may help to discover more intriguing physics in correlated and topological quantum materials.

ACKNOWLEDGMENTS

We thank Y. Wu, J. Li, K. Jiang, J. Hu, F. Zhang, Z. Han, X. Lu, and S. Zhang for valuable discussions. This work is supported by the National Natural Science Foundation of China (Grant No. 12174257), the National Key R & D program of China (Grant No. 2020YFA0309601), and the start-up grant of ShanghaiTech University.

[1] D. L. Bergman, C. Wu, and L. Balents, Phys. Rev. B **78**, 125104 (2008).
[2] E. Tang, J.-W. Mei, and X.-G. Wen, Phys. Rev. Lett. **106**, 236802 (2011).
[3] M. L. Kiesel, C. Platt, and R. Thomale, Phys. Rev. Lett. **110**, 126405 (2013).
[4] W.-S. Wang, Z.-Z. Li, Y.-Y. Xiang, and Q.-H. Wang, Phys. Rev. B **87**, 115135 (2013).
[5] M. L. Kiesel and R. Thomale, Phys. Rev. B **86**, 121105 (2012).
[6] S.-L. Yu and J.-X. Li, Phys. Rev. B **85**, 144402 (2012).
[7] J.-X. Yin, S. S. Zhang, H. Li, K. Jiang, G. Chang, B. Zhang, B. Lian, C. Xiang, I. Belopolski, H. Zheng *et al.*, Nature (London) **562**, 91 (2018).
[8] L. Ye, M. Kang, J. Liu, F. Von Cube, C. R. Wicker, T. Suzuki, C. Jozwiak, A. Bostwick, E. Rotenberg, D. C. Bell *et al.*, Nature (London) **555**, 638 (2018).
[9] E. Liu, Y. Sun, N. Kumar, L. Muechler, A. Sun, L. Jiao, S.-Y. Yang, D. Liu, A. Liang, Q. Xu *et al.*, Nat. Phys. **14**, 1125 (2018).
[10] J.-X. Yin, W. Ma, T. A. Cochran, X. Xu, S. S. Zhang, H.-J. Tien, N. Shumiya, G. Cheng, K. Jiang, B. Lian *et al.*, Nature (London) **583**, 533 (2020).
[11] W.-H. Ko, P. A. Lee, and X.-G. Wen, Phys. Rev. B **79**, 214502 (2009).
[12] L. Balents, Nature (London) **464**, 199 (2010).
[13] B. R. Ortiz, L. C. Gomes, J. R. Morey, M. Winiarski, M. Bordelon, J. S. Mangum, I. W. H. Oswald, J. A. Rodriguez-Rivera, J. R. Neilson, S. D. Wilson, E. Ertekin, T. M. McQueen, and E. S. Toberer, Phys. Rev. Mater. **3**, 094407 (2019).
[14] S.-Y. Yang, Y. Wang, B. R. Ortiz, D. Liu, J. Gayles, E. Derunova, R. Gonzalez-Hernandez, L. vSmejkal, Y. Chen, S. S. Parkin *et al.*, Sci. Adv. **6**, eabb6003 (2020).
[15] Y.-X. Jiang, J.-X. Yin, M. M. Denner, N. Shumiya, B. R. Ortiz, G. Xu, Z. Guguchia, J. He, M. S. Hossain, X. Liu *et al.*, Nat. Mater. **20**, 1353 (2021).
[16] H. Li, S. Wan, H. Li, Q. Li, Q. Gu, H. Yang, Y. Li, Z. Wang, Y. Yao, and H.-H. Wen, Phys. Rev. B **105**, 045102 (2022).
[17] F. H. Yu, T. Wu, Z. Y. Wang, B. Lei, W. Z. Zhuo, J. J. Ying, and X. H. Chen, Phys. Rev. B **104**, L041103 (2021).
[18] Z. Liang, X. Hou, F. Zhang, W. Ma, P. Wu, Z. Zhang, F. Yu, J.-J. Ying, K. Jiang, L. Shan *et al.*, Phys. Rev. X **11**, 031026 (2021).
[19] H. Zhao, H. Li, B. R. Ortiz, S. M. Teicher, T. Park, M. Ye, Z. Wang, L. Balents, S. D. Wilson, and I. Zeljkovic, Nature (London) **599**, 216 (2021).
[20] H. Li, Y.-X. Jiang, J. X. Yin, S. Yoon, A. R. Lupini, C. Nelson, A. Said, Y. M. Yang, H. Lei, B. Yan *et al.*, arXiv:2109.03418 (2021).
[21] Z. Wang, Y.-X. Jiang, J.-X. Yin, Y. Li, G.-Y. Wang, H.-L. Huang, S. Shao, J. Liu, P. Zhu, N. Shumiya *et al.*, Phys. Rev. B **104**, 075148 (2021).
[22] B. R. Ortiz, S. M. L. Teicher, L. Kautzsch, P. M. Sarte, N. Ratcliff, J. Harter, J. P. C. Ruff, R. Seshadri, and S. D. Wilson, Phys. Rev. X **11**, 041030 (2021).
[23] K. Nakayama, Y. Li, T. Kato, M. Liu, Z. Wang, T. Takahashi, Y. Yao, and T. Sato, Phys. Rev. B **104**, L161112 (2021).
[24] H. Li, H. Zhao, B. R. Ortiz, T. Park, M. Ye, L. Balents, Z. Wang, S. D. Wilson, and I. Zeljkovic, Nat. Phys. **18**, 265 (2022).
[25] M. Kang, S. Fang, J.-K. Kim, B. R. Ortiz, S. H. Ryu, J. Kim, J. Yoo, G. Sangiovanni, D. Di Sante, B.-G. Park *et al.*, Nat. Phys. **18**, 301 (2022).
[26] Y. Xiang, Q. Li, Y. Li, W. Xie, H. Yang, Z. Wang, Y. Yao, and H.-H. Wen, Nat. Commun. **12**, 6727 (2021).
[27] Z. Wang, S. Ma, Y. Zhang, H. Yang, Z. Zhao, Y. Ou, Y. Zhu, S. Ni, Z. Lu, H. Chen *et al.*, arXiv:2104.05556 (2021).
[28] Z. Liu, N. Zhao, Q. Yin, C. Gong, Z. Tu, M. Li, W. Song, Z. Liu, D. Shen, Y. Huang *et al.*, Phys. Rev. X **11**, 041010 (2021).
[29] S. Cho, H. Ma, W. Xia, Y. Yang, Z. Liu, Z. Huang, Z. Jiang, X. Lu, J. Liu, Z. Liu *et al.*, Phys. Rev. Lett. **127**, 236401 (2021).
[30] X. Zhou, Y. Li, X. Fan, J. Hao, Y. Dai, Z. Wang, Y. Yao, and H.-H. Wen, Phys. Rev. B **104**, L041101 (2021).
[31] Y. Xie, Y. Li, P. Bourges, A. Ivanov, Z. Ye, J.-X. Yin, M. Z. Hasan, A. Luo, Y. Yao, Z. Wang *et al.*, Phys. Rev. B **105**, L140501 (2022).
[32] D. Wulferding, S. Lee, Y. Choi, Q. Yin, Z. Tu, C. Gong, H. Lei,

S. Yousuf, J. Song, H. Lee, T. Park, and K.-Y. Choi, Phys. Rev. Res. **4**, 023215 (2022).
[33] Z. X. Wang, Q. Wu, Q. W. Yin, C. S. Gong, Z. J. Tu, T. Lin, Q. M. Liu, L. Y. Shi, S. J. Zhang, D. Wu *et al.*, Phys. Rev. B **104**, 165110 (2021).
[34] B. Q. Song, X. M. Kong, W. Xia, Q. W. Yin, C. P. Tu, C. C. Zhao, D. Z. Dai, K. Meng, Z. C. Tao, Z. J. Tu *et al.*, arXiv:2105.09248 (2021).
[35] C. Mielke, D. Das, J.-X. Yin, H. Liu, R. Gupta, Y.-X. Jiang, M. Medarde, X. Wu, H. C. Lei, J. Chang *et al.*, Nature (London) **602**, 245 (2022).
[36] L. Yu, C. Wang, Y. Zhang, M. Sander, S. Ni, Z. Lu, S. Ma, Z. Wang, Z. Zhao, H. Chen *et al.*, arXiv:2107.10714 (2021).
[37] Q. Wu, Z. Wang, Q. Liu, R. Li, S. Xu, Q. Yin, C. Gong, Z. Tu, H. Lei, T. Dong *et al.*, arXiv:2110.11306 (2021).
[38] L. Nie, K. Sun, W. Ma, D. Song, L. Zheng, Z. Liang, P. Wu, F. Yu, J. Li, M. Shan *et al.*, Nature (London) **604**, 59 (2022).
[39] B. R. Ortiz, P. M. Sarte, E. M. Kenney, M. J. Graf, S. M. L. Teicher, R. Seshadri, and S. D. Wilson, Phys. Rev. Mater. **5**, 034801 (2021).
[40] Q. Yin, Z. Tu, C. Gong, Y. Fu, S. Yan, and H. Lei, Chin. Phys. Lett. **38**, 037403 (2021).
[41] B. R. Ortiz, S. M. L. Teicher, Y. Hu, J. L. Zuo, P. M. Sarte, E. C. Schueller, A. M. Abeykoon, M. J. Krogstad, S. Rosenkranz, R. Osborn, R. Seshadri, L. Balents, J. He, and S. D. Wilson, Phys. Rev. Lett. **125**, 247002 (2020).
[42] K. Y. Chen, N. N. Wang, Q. W. Yin, Y. H. Gu, K. Jiang, Z. J. Tu, C. S. Gong, Y. Uwatoko, J. P. Sun, H. C. Lei, J. P. Hu, and J. G. Cheng, Phys. Rev. Lett. **126**, 247001 (2021).
[43] Z. Zhang, Z. Chen, Y. Zhou, Y. Yuan, S. Wang, J. Wang, H. Yang, C. An, L. Zhang, X. Zhu *et al.*, Phys. Rev. B **103**, 224513 (2021).
[44] X. Chen, X. Zhan, X. Wang, J. Deng, X.-B. Liu, X. Chen, J.-G. Guo, and X. Chen, Chin. Phys. Lett. **38**, 057402 (2021).
[45] H. Li, T. T. Zhang, T. Yilmaz, Y. Y. Pai, C. E. Marvinney, A. Said, Q. W. Yin, C. S. Gong, Z. J. Tu, E. Vescovo *et al.*, Phys. Rev. X **11**, 031050 (2021).
[46] C. Zhao, L. Wang, W. Xia, Q. Yin, J. Ni, Y. Huang, C. Tu, Z. Tao, Z. Tu, C. Gong *et al.*, arXiv:2102.08356 (2021).
[47] R. Gupta, D. Das, C. H. Mielke III, Z. Guguchia, T. Shiroka, C. Baines, M. Bartkowiak, H. Luetkens, R. Khasanov, Q. Yin *et al.*, Npj Comput. Mater. **7**, 49 (2022).
[48] H.-S. Xu, Y.-J. Yan, R. Yin, W. Xia, S. Fang, Z. Chen, Y. Li, W. Yang, Y. Guo, and D.-L. Feng, Phys. Rev. Lett. **127**, 187004 (2021).
[49] F. Yu, D. Ma, W. Zhuo, S. Liu, X. Wen, B. Lei, J. Ying, and X. Chen, Nat. Commun. **12**, 3645 (2021).
[50] R. Lou, A. Fedorov, Q. Yin, A. Kuibarov, Z. Tu, C. Gong, E. F. Schwier, B. Büchner, H. Lei, and S. Borisenko, Phys. Rev. Lett. **128**, 036402 (2022).
[51] S. Ni, S. Ma, Y. Zhang, J. Yuan, H. Yang, Z. Lu, N. Wang, J. Sun, Z. Zhao, D. Li *et al.*, Chin. Phys. Lett. **38**, 057403 (2021).
[52] H. Chen, H. Yang, B. Hu, Z. Zhao, J. Yuan, Y. Xing, G. Qian, Z. Huang, G. Li, Y. Ye *et al.*, Nature (London) **599**, 222 (2021).
[53] L. Yin, D. Zhang, C. Chen, G. Ye, F. Yu, B. R. Ortiz, S. Luo, W. Duan, H. Su, J. Ying *et al.*, Phys. Rev. B **104**, 174507 (2021).
[54] Y. Gu, Y. Zhang, X. Feng, K. Jiang, and J. Hu, Phys. Rev. B **105**, L100502 (2022).
[55] T. Park, M. Ye, and L. Balents, Phys. Rev. B **104**, 035142 (2021).
[56] X. Wu, T. Schwemmer, T. Müller, A. Consiglio, G. Sangiovanni, D. Di Sante, Y. Iqbal, W. Hanke, A. P. Schnyder, M. M. Denner *et al.*, Phys. Rev. Lett. **127**, 177001 (2021).
[57] M. M. Denner, R. Thomale, and T. Neupert, Phys. Rev. Lett. **127**, 217601 (2021).
[58] H. Miao, H. X. Li, W. R. Meier, A. Huon, H. N. Lee, A. Said, H. C. Lei, B. R. Ortiz, S. D. Wilson, J. X. Yin, M. Z. Hasan, Z. Wang, H. Tan, and B. Yan, Phys. Rev. B **104**, 195132 (2021).
[59] Y.-P. Lin and R. M. Nandkishore, Phys. Rev. B **104**, 045122 (2021).
[60] X. Feng, K. Jiang, Z. Wang, and J. Hu, Sci. Bull. **66**, 1384 (2021).
[61] A. Consiglio, T. Schwemmer, X. Wu, W. Hanke, T. Neupert, R. Thomale, G. Sangiovanni, and D. Di Sante, Phys. Rev. B **105**, 165146 (2022).
[62] Z. Ye, A. Luo, J.-X. Yin, M. Z. Hasan, and G. Xu, Phys. Rev. B **105**, 245121 (2022).
[63] H. Tan, Y. Liu, Z. Wang, and B. Yan, Phys. Rev. Lett. **127**, 046401 (2021).
[64] C. Wang, S. Liu, H. Jeon, and J.-H. Cho, Phys. Rev. B **105**, 045135 (2022).
[65] K. Jiang, T. Wu, J.-X. Yin, Z. Wang, M. Z. Hasan, S. D. Wilson, X. Chen, and J. Hu, arXiv:2109.10809 (2021).
[66] X. Feng, Y. Zhang, K. Jiang, and J. Hu, Phys. Rev. B **104**, 165136 (2021).
[67] N. Ratcliff, L. Hallett, B. R. Ortiz, S. D. Wilson, and J. W. Harter, Phys. Rev. Mater. **5**, L111801 (2021).
[68] X. Ren, P. Rinke, C. Joas, and M. Scheffler, J. Mater. Sci. **47**, 7447 (2012).
[69] M. M. Korshunov, Phys. Usp. **57**, 813 (2014).
[70] G. Kresse and J. Furthmüller, Phys. Rev. B **54**, 11169 (1996).
[71] J. P. Perdew, K. Burke, and M. Ernzerhof, Phys. Rev. Lett. **77**, 3865 (1996).
[72] D. Vanderbilt, Phys. Rev. B **41**, 7892 (1990).
[73] A. A. Mostofi, J. R. Yates, Y.-S. Lee, I. Souza, D. Vanderbilt, and N. Marzari, Comput. Phys. Commun. **178**, 685 (2008).
[74] J. Kanamori, Prog. Theor. Phys. **30**, 275 (1963).
[75] A. Georges, L. d. Medici, and J. Mravlje, Annu. Rev. Condens. Matter Phys. **4**, 137 (2013).
[76] See Supplemental Material at http://link.aps.org/supplemental/10.1103/PhysRevB.106.155125 for: (a) more results for the bare and RPA susceptibility calculations for AV_3Sb_5 (A = K, Rb, Cs), (b) formalism and more results of Hartree-Fock calculations in the pristine structure, $2 \times 2 \times 1$ supercell, and $2 \times 2 \times 2$ supercell for AV_3Sb_5 (A = K, Rb, Cs), (d) details about the calculations for the intersite currents, (e) details about anomalous Hall conductivity calculations, and (f) results of Hartree-Fock calculations with different interaction parameters.
[77] J. Liu and L. Balents, Phys. Rev. B **95**, 075426 (2017).
[78] A. Uehara, H. Shinaoka, and Y. Motome, Phys. Rev. B **92**, 195150 (2015).
[79] W.-X. Qiu, J.-Y. Zou, A.-Y. Luo, Z.-H. Cui, Z.-D. Song, J.-H. Gao, Y.-L. Wang, and G. Xu, Phys. Rev. Lett. **127**, 147202 (2021).
[80] J. Rath and A. J. Freeman, Phys. Rev. B **11**, 2109 (1975).
[81] J. Zhao, W. Wu, Y. Wang, and S. A. Yang, Phys. Rev. B **103**, L241117 (2021).
[82] H. Ishizuka and N. Nagaosa, Phys. Rev. B **103**, 235148 (2021).
[83] F. Giustino, Rev. Mod. Phys. **89**, 015003 (2017).